NIST-GCR-94-648

UPWARD FLAME SPREAD ALONG THE VERTICAL CORNER WALLS

C. Qian, H. Ishida, and K. Saito
Department of Mechanical Engineering
University of Kentucky
Lexington, KY 40506

Issued June 1994
October 1993

Sponsored by:
U.S. Department of Commerce
Ronald H. Brown, *Secretary*
Technology Administration
Mary L. Good, *Under Secretary for Technology*
National Institute of Standards and Technology
Arati Prabhakar, *Director*

Notice

This report was prepared for the Building and Fire Research Laboratory of the National Institute of Standards and Technology under grant number 60NANB2D1295. The statements and conclusions contained in this report are those of the authors and do not necessarily reflect the views of the National Institute of Standards and Technology or the Building and Fire Research Laboratory.

UPWARD FLAME SPREAD ALONG THE VERTICAL CORNER WALLS

Cheng Qian, Hiroki Ishida and Kozo Saito

Combustion and Fire Research Laboratory
Department of Mechanical Engineering
University of Kentucky
Lexington, KY 40506

ABSTRACT

Flame spread behavior and the pyrolysis region spread characteristics along vertical corner walls were studied in detail with an automated infrared imaging temperature measurement technique (IR technique). The technique was recently developed for the measurement of transient pyrolysis temperature on both charring and non–charring materials. Temporal isotherms on PMMA samples were successfully obtained, from which the progress rate of the pyrolysis front was automatically deduced. It was found that the pyrolysis front shape was always M–shaped, i.e., no spread along the corner, and the maximum spread is in a few centimeters away from the corner. Understanding of the mechanism of the M–shape formation is important in developing a prediction model of the spread rate. Four possible mechanisms were identified and flame displacement effects are found to be the principal mechanism. Transient total heat flux distributions above the M–shape pyrolysis peak for a spreading fire were measured. Using these values, it was shown that the upward spread rate is predictable from a simple, one–dimensional, thermal model.

Nomenclature

T_{ig}	ignition temperature
T_s	surface temperature
t_f	time for flame tip reaching flux meter
t_p	time for pyrolysis front reaching flux meter
U_p	vertical flame spread rate
V_p	horizontal flame spread rate
X_p	pyrolysis height at the peak
x_p	pyrolysis height
Y_p	pyrolysis width at the bottom
y_p	pyrolysis width
Y_o	length of ignition line
Y_p	pyrolysis width at the bottom
ξ	normalized pyrolysis height
η	normalized pyrolysis width
ϕ	heat transfer parameter

INTRODUCTION

Upward flame spread is an important subject in fire safety engineering because of its rapid fire growth rate and intense radiant emission from the flame. In the past, both theoretical and experimental research on upward flame spread, along a vertically oriented flat wall, have been published [1–8]. In these studies, a one–dimensional spread rate model is employed, assuming that two dimensional flame spread behavior is sustained with reasonable accuracy. The modeling of upward flame spread along vertically oriented corner walls, however, requires additional considerations due to the transient three–dimensional nature of the fire–induced flow [9–11]. Williamson, et al. [9] reported that a complex "T shape pattern" as the characteristic flame spread behavior in room corner fires. Because of the complex nature of the fire–induced flow and of spread pattern, there are only a few prediction models proposed for corner fires. One of these examples will be the Quintiere model [12] which is composed of concurrent–flow assisted vertical spread and opposed–flow assisted horizontal spread. The model is simple, and needs to be tested against experiments to determine whether or not it is of practical usefulness.

The goal of this research project is to provide a reliable data base on which prediction models can be constructed, and to develop a simple and practical prediction model. To that end, we designed a one–half scale room corner model and conducted a series of flow visualization experiments [10]. Three different types of visualization techniques were applied to increase the reliability. One of major findings of this test is the sporadic formation of a vortex tube which sometimes traveled to ceiling. An IR technique was also developed previously to accurately measure the location of pyrolysis front [11], since the conventional thermocouple technique has limitations on the measurement of the pyrolysis front spread rate in complex geometry room fires such as

corner–wall fires.

A series of corner wall fires were conducted with PMMA corner walls. It was found that the behavior of the flame and the spread pattern of the pyrolysis front were affected by the initial mode of ignition at the bottom of corner walls; namely the location and the area of ignition at the bottom. In this report, flame spread in a line ignition mode with various lengths along the bottom edge are studied. A series of upward flame spread tests along the vertically oriented PMMA corner walls were conducted. The spread rate of the pyrolysis front region was successfully measured using the IR technique.

We report here: (1) Experimental findings in characteristics of spreading flame behavior and the pyrolysis front shape on the corner wall fires which includes total heat flux measurement on PMMA wall surface for spreading fires and measurement of relative height of the visible flame tip and pyrolysis front; (2) The mechanism of the M–shape pyrolysis front formation; (3) the applicability of the one–dimensional thermal model to predict the upward spread rate, along the vertical corner walls; and (4) Heat flux distributions on the wall with and without ceiling (see Apendix). The above (2) and (3) tasks are the alternation for the task 3 – Quantification of fire–induced flow, in the original proposal. The alternation was needed after the project was started, since we realized the (2)–(3) results are so important to complete the principal objective of this project. However, the projection was not clear at the time when the proposal was submitted.

EXPERIMENTAL METHODS

Infrared Imaging Temperature Measurement

For the measurement of transient temperature profiles of the unburned wall surface, conventional thermocouple techniques have limitations due to the complexity of implementation and the uncertainty of pyloysis temperature of the wall surface

(particularly for charring materials) [3,4]. Visual observation techniques which have been applied previously for spread rate measurement [1,3–4] can produce ambiguous results in the determination of the two–dimensional transient pyrolysis front location. To overcome the limitations associated with these conventional methods, infrared radiometry, which is very useful for non–contact surface temperature measurement [13,14], was applied with automated image analysis to obtain transient surface temperature distributions. In a previous study [11], the infrared camera was located away from the fire source and it must measure the wall temperature through the flame. The main difficulty was that the wall temperature (approximately 600 K) is considerably lower than the flame temperature, and thus the flame radiation causes interference, i.e. the infrared system would detect some intermediate flame temperature instead of the wall temperature. To avoid flame interference which includes radiation from solid soot particles and excited gas molecules, several narrow band pass filters were used with the infrared camera. It was found that the infrared image through a 10.8 ± 0.5 μm band–pass filter had no flame interference effects, and accurately represent the wall temperature. Theoretical considerations confirmed that the technique is applicable for the spread rate measurement along commonly used building materials.

Comparison of Thermocouple and IR Data

To ensure that the IR technique is applicable for the materials whose emissivity changes during pyrolysis, a further experiment was conducted using a PMMA sample. Figure 1 shows surface temperature histories during upward flame spread. The measurement was done along the center of a vertically oriented PMMA sample, 45 cm high x 12 cm wide x 1.2 cm thick, with a 0.07 mm diameter chromel–alumel thermocouple and the IR camera. The emissivity set up for the IR camera was based upon the previous study [11]. The results show that the pyrolysis front temperature, 370

^{o}C determined by the thermocouple, corresponds to that determined by the infrared camera, 329 ^{o}C. To understand the difference between the two measurements and structure of the pyrolysis front, the pyrolysis front location was examined as follows. The spreading flame was extinguished by applying a sudden purge of CO_2 when the infrared image achieved a temperature of 329 ^{o}C, at a specified location of the sample surface. On the extinguished sample surface, the pyrolysis front location was identified as a clear boundary between the thermally damaged region where fine bubbled surface with soot deposits occurred, and the undamaged surface darkened with soot deposits. The temperature contour of 329 ^{o}C obtained by the infrared image exactly matched the boundary. On the other hand, the determination of the pyrolysis front location is not obvious when the thermocouple data were used. Usually the pyrolysis front is determined by the first maximum peak in the surface temperature history, which was 370 ^{o}C in this experiment. During the pyrolysis process, however, the PMMA surface softens, melts and forms fine bubbles, affecting the relative location of the thermocouple bead to the original surface. Therefore, careful interpretation is needed when the thermocouple is used for pyrolysis front measurement [11]. In contrast, the infrared imaging temperature measurement technique, a non–intrusive technique, does not possess these problems.

Upward Flame Spread along the Vertical Corner Walls

As shown in Fig. 2, the PMMA samples were flush–mounted and fixed to large Marinite walls housed in the one–half scale room corner model (1.6 m high x 1.0 m wide x 1.0 m long) with a Marinite ceiling and a Marinite floor. The infrared camera was located away from the fire source to acquire the wall temperature through the flame. The obtained infrared images can be transformed into two–dimensional images using a previously developed technique [11]. The PMMA corner walls were ignited at a spot on the corner bottom and/or at some distance along the bottom, by a small propane torch.

This was done to provide the sample with the minimum ignition energy in a relatively short period of time, preventing excess preheat of the virgin material. The time series of the wall temperature distribution was obtained using the IR camera with the 10.8 ± 0.5 μm band–pass filter. The visible flame shape was simultaneously recorded by a video camera, from which a time averaged visible flame height was obtained. When the pyrolysis front reached the top of the sample, the flame was extinguished by a sudden purge of CO_2 for the measurement of the pyrolysis shape and the examination of the sample surface.

RESULTS AND DISCUSSION

Mechanism of the M–shape Pyrolysis Front Formation

Figure 3 shows the infrared pyrolysis front (329 ^{o}C iso–therm) measured at six different time periods after ignition (t = 0). The formation of the M–shape pyrolysis front is evident; and the spread rate, in any direction, can readily be deduced from this result. If an attempt was made to duplicate the similar result by multi–point thermocouple measurement, the work will be extremely elaborate.

From the fire safety point of view, the prediction of the maximum upward spread rate is crucial. However, spread rate predictions for the tip of the M–shape pyrolysis front may be difficult, since it is related to three dimensional fire–induced flow which sometimes accompanies sporadic formation of vortex tubes as observed previously in our laboratory using smoke streak and particle track techniques [10]. To develop a model to predict the upward spread rate, it is important to understand the mechanism of the M–shape pyrolysis front formation, since its peak spreads toward the ceiling with the maximum rate. The following four mechanisms, mechanisms M–1 through M–4 were considered.

M–1 Effect of Ignition Mode

In the first series of experiments, the bottom of both corner walls was uniformly ignited by a propane torch. After uniform line ignition occurred, a sustained upward flame spread followed. The temporal infrared–images over the PMMA sample surface were obtained using the IR camera. Both the infrared image and the extinguished sample surface resulted in a distinguished M–shape pyrolysis front on the sample surface.

In the second series of ignition experiments, a spot ignition was provided at the bottom corner, allowing the flame to spread horizontally and vertically. In the third series of ignition experiments, a line ignition was provided at the bottom of only one side wall. The same experimental methods were applied for the measurement of pyrolysis front shape. However, for both cases the M–shape pyrolysis front occurred and those results are schematically shown in Figs. 4 and 5. The shape of the M–shape differs slightly depending on the ignition mode, but the occurrence of the M–shape formation was still sustained. Interestingly, Fig. 5 – a representative flame behavior and the shape of pyrolysis front plot, shows that the height of pyrolysis region on the initially torch–ignited wall is shorter than that on the unignited wall, resulting in the fastest spread over the initially unignited wall. This may be attributed to the fact that for the initially unignited wall, enhanced convective heat transfer occurred through a steeper temperature gradient, which was formed near the unignited wall, due to the closer distance between the flame and the wall. Visual observation and gas phase temperature measurements proved that is the case.

M–2 Effect of Solid Phase Conduction Heat Loss

Based on the failure of the M–1 mechanism, conduction heat through the corner wall was thought to be the main reason for the M–shape pyrolysis front formation [15]. To test this mechanism, two different corner configurations, as shown in Fig. 6 (case I

and case II), were designed. In the case I, two PMMA samples were glued together to form a solid corner; while in the case II, two PMMA samples were fixed to form a hollow corner. For case I, a large conduction heat loss is expected through the solid corner wall, while for the case II, a minimal conduction loss was expected. In addition, two PMMA samples were fixed with a 1 cm distance between each sample with the intention to test the M–3 mechanism to be explained later.

The three models are composed of two same size pieces of PMMA wall, 1 m high x 30 cm wide x 2 cm thick. These samples were fixed against large Marinite walls and a uniform line ignition was provided along the bottom of the sample by the propane torch. Several minutes after a saturated upward spread occurred, the flame tip reached the ceiling. The flame was then extinguished by a sudden purge of CO_2 and the pyrolysis front shape was measured as previously described.

If the M–2 mechanism is the principal reason for the M–shape pyrolysis front formation, it is expected that the pyrolysis front shape for cases I and II should be significantly different (the case II pyrolysis shape is not likely the M–shape). However, the two cases resulted in a very similar M–shape, as shown in Fig. 6, rejecting the above assumption.

M–3 Fire–induced Flow Cooling

The fire–induced air may be entrained through the bottom (or possibly from top) of the corner and it may flow along the corner. If a substantial amount of the air flow is entrained, a significant cooling effect could be expected. The possibility of this mechanism, suggested by Williams [16] is certainly worth examining, since the previous flow visualization results [10] revealed a sporadic vortex formation along the corner. To examine this mechanism, a case III experiment was designed and performed using the same experimental method as applied to testing the M–2 mechanism.

The intention of this experiment is to significantly reduce (or possibly eliminate) the fire–induced flow along the corner by separating the two samples by 1 cm, the distance sufficiently smaller than the distance between the corner and the pyrolysis front peak. Under these experimental conditions, a significant change in the pyrolysis front shape is expected, if M–3 is the principal mechanism. However, case III experiments resulted in an M–shape formation, similar to that of the case I. When the two walls were further separated, flame spread becomes similar to the single vertical wall case, as it is expected.

To further confirm the insignificance of the M–3 effect, a square piece of aluminum, 5 cm long x 5 cm wide x 0.5 cm thick, was placed on the corner halfway between the sample top and the bottom and normal to the corner walls. The disk is large enough to alter and/or stop the flow, yet small enough to cause an insignificant heat loss effect. The same experimental method, applied to the M–2 experiment, was also applied to this experiment and again a positive result (formation of M–shape pyrolysis front) appeared. A schematic of the pyrolysis shape is shown in Fig. 7

M–4 Flame Displacement Effect

Because of the unsuccessful trials with the mechanisms M–1 through M–3, the M–4 mechanism – flame displacement effect, was finally considered. This mechanism is based on a large heat loss in the gas phase due to poor mixing of pyrolysis products and air forming a nonflammable (probably fuel rich mixture) layer between the corner and the flame. The thickness of this layer is large enough to cause significant conductive and convective heat losses in the gas phase, so that the corner temperature does not reach pyrolysis temperature.

Through a series of simple exploratory tests, it was found that the flame displacement distance, the distance between the flame sheet location (the location of the

maximum temperature) and the wall corner can change by changing corner angle, θ. To further investigate this observation, three different corner–angle models were designed and schematics of these models are shown in Fig. 8. Three corner models ($\theta = 45^{o}$, 90^{o} and 135^{o}) are composed of two PMMA walls; each wall has dimensions of 1 m high x 30 cm wide x 2 cm thick. The $\theta = 180^{o}$ model is made of a single PMMA sheet with the same dimension. A one–half scale room corner apparatus [10,11] designed in the Combustion and Fire Research laboratory at the University of Kentucky (Fig. 2), was used for this experiment. During flame spread, the IR camera was used to measure the temporal pyrolysis location. Flame displacement distance δ was defined as the minimum distance from the corner to the maximum temperature location, which was determined by traversing a 100 μm diameter, alumel–chromel thermocouple normal to the corner. After a steady state spread was achieved and the pyrolysis front reached half way to the top, the flame was extinguished by a sudden purge of CO_2. The pyrolysis shape was clearly identified on the extinguished PMMA surface, and schematics of it are shown in Fig. 8. Of particular interest is Fig. 8c, the $\theta = 135^{o}$ case, which resulted in no M–shape formation. Fig. 8a shows somewhat enhanced image of the M–shape, while Fig. 8d shows a parabolic shape pyrolysis front normally approximated as a one–dimensional spread [3,4].

Flame Spread Rates and a Similarity Model for Pyrolysis Front

Typically, a fire ignited on a section of a corner wall spreads vertically and horizontally. Different ignition methods correspond to various spread modes. The effect of unsymmetrical ignition (one side ignition) has been discussed [17]. This study reports the fire spread phenomena in a symmetric line ignition mode along the bottom of corner walls. When the PMMA corner walls are ignited on both sides symmetrically, and the height of ignition zone is fixed (3cm), then the length of ignition zone Y_0 is the only

controlling parameter for this simulated fire scenario. During flame spread, an M–shaped pyrolysis front was formed as explained earlier. It was found that the vertical spread rate increased with increasing ignition length to 20cm, and then remained constant up to 40cm [18]. In the current experiment, a full size sample, that expands from the floor to the ceiling with a PMMA ceiling, was tested. Interestingly, when the upwardly spreading pyrolysis front reached the height of 140cm, the top of the corner wall and part of ceiling were already ignited allowing a simultaneous downward spread (Fig. 9). Because of this, fire growth rate increased significantly.

In the M–shaped pyrolysis front spread mode, vertical spread at the peak and horizontal spread at the base are critical aspects of the flame spread phenomena. As pointed out by Quintiere [12] and experimentally observed by our group [18], the vertical flame spread is a concurrent flow spread (in the direction of local gas flow) and horizontal flame spread is an opposed flow spread (opposite to the local gas flow). These spread characteristics are discussed separately as follows.

(a) Vertical Flame Spread at the Peak

The peak heights of pyrolysis front, X_p, detected by IR camera as a function of time for three ignition lengths (Y_o = 20, 30 and 40 cm), are presented in Fig. 10. There is a good agreement for the results from the three tests when $X_p > 20$cm. By the observation, the disagreement in the region $X_p < 20$cm corresponds to the transition from laminar flame spread to turbulent, and with the effects of ignition. We also found that X_p varies almost linearly with time for $X_p > 20$cm in this plot. This linear distribution suggests an exponentially increasing pyrolysis height as a function of time. A least–square logarithmic fit of the data for pyrolysis heights above X_p = 20cm yields

$$X_p = 0.003t^{1.84} \qquad (1)$$

Figure 11 shows the upward spread rate as a function of pyrolysis height for the data from the three experiments. A similar scale flat wall test result [1] conducted by FRMC group is also compared in the figure. In both cases, the spread rate is essentially proportional to pyrolysis height, but the upward spread rate for the corner fires is about three times faster than that for the same scale vertical flat wall fire, i.e., $V_p = 0.0134X_p^{0.944}$ for the corner fires versus $V_p = 0.00441X_p^{0.964}$ for the flat wall fires. The high spread rate is mainly contributed to a strong fire induced flow that enhanced heat convection from the flame to the wall surface and an enhanced radiation from the flame to the walls. There exists a critical ignition length (approximately 20cm in our experiment) beyond which flame spread rate does not increase, probably because the fire induced flow in the corner may not be enhanced further due to a cellular structure of diffusion flames [3].

(b) Horizontal Spread at the Base

From Quintiere et al [5], downward and lateral flame spread in air, on a vertical flat wall can be expressed as follows:

$$V_p = \frac{\phi}{(k\rho c)\ (T_{ig} - T_s)^2} \qquad (2)$$

where they found ignition temperature $T_{ig} = 378\ ^oC$, effective thermal inertia $k\rho c = 1.02\ (kW/m^2K)^2s$ and flame heat transfer parameter $\phi = 14.4\ (kW)^2/m^3$ for PMMA. From previous corner fire experimental results [19], $V_p = 0.0113$ cm/s. By equation (2), it can be obtained that $\phi = 12.0\ (kW)^2/m^3$; therefore, the heat transfer parameters for these two cases are very close. The resulting good agreement may be attributed to the fact that the additional radiant heat flux from the other side wall and flame is offset by a stronger

opposed flow confined by corner walls. A similar mechanism that causes the approximate constant lateral spread rate with increasing ignition length was discussed earlier. Hence the width of the pyrolysis region as a function of time at the base can be given as,

$$Y_p = 0.0113t + Y_o \tag{3}$$

(c) The Similarity Model for Pyrolysis Front on Corner Wall

The location of spreading pyrolysis front was measured by the IR camera as a function of time and is shown in Fig. 12(a). To find a similarly fit of the geometry of the pyrolysis region, the data was normalized by the peak pyrolysis height, X_p, and by the base pyrolysis width, Y_p, respectively in vertical and horizontal direction. The normalized data correlation for $X_p > 20$cm is excellent as shown in Fig. 12(b). A normalized pyrolysis front fit was then made using a fifth order polynomial with a correlation coefficient of 0.993. Hence an empirical model for the pyrolysis front was obtained as:

$$\xi = 32.74\eta^5 - 107.24\eta^4 + 127.87\eta^3 - 67.30\eta^2 + 14.0\eta + 0.02 \tag{4}$$

where, $\xi = x_p/X_p = x_p/0.003t^{1.84}$ and $\eta = y_p/Y_p = y_p/(0.0113t + Y_o)$

(2) Heat Flux from the Flame and a One–Dimensional Heat Transfer Model to Predict Spread Rate

A first step has been taken to characterize the heat transfer process in the preheat region, so that the upward flame spread rate might be predicted. Heat flux test was performed with a 160 cm high PMMA corner model with an ignition length of 20 cm on

each side of the corner wall bottom. Total heat flux histories were measured at five different positions distributed along the trajectory of the pyrolysis peak, located in previous experiment. Figure 13 shows the measured incident total heat flux versus time and distance from the bottom, where t_f and t_p respectively correspond to the times when the flame tip and pyrolysis front reach the measuring point. There is no significant increase in heat flux when the flame begins to cover the measuring point, so a visible flame height is probably not ideal parameter to consider as a preheat characteristic length for corner fires (this assumption is usually made for flame spread over a vertical flat wall [1, 3]). A maximum heat flux of 3.25 W/cm^2 was achieved in the pyrolysis zone that is approximately 50–60% higher than the flat wall values.

To understand the heat transfer process, we assume lateral heat diffusion inside the sample can be neglected, i.e. a one–dimensional heat conduction model is applicable in the preheat region. Using the formula from [20], the surface temperature of a semi–infinite slab initially at the uniform temperature T_0, subjected to a net heating flux $q''(x,t)$ can be given by

$$T_s(x,t) = T_0 + \frac{1}{\sqrt{\pi k \rho c}} \int_0^t \frac{q''(x,t)}{\sqrt{t-\tau}}\, d\tau \qquad (5)$$

By equation (5), which was also used by Mitler in his upward flame spread model [2], the time when the pyrolysis front reaches the heat flux measurement height can be computed based on the measured incident heat flux history in the preheat period (from $t = 0$ to t_p). For this purpose the heat flux history ($0 < t < t_p$) was approximated by a third order polynomial fit, and then introduced into equation (5). In Fig. 14, the calculated pyrolysis height was plotted as a function of time and compared with the measured data with a reasonable agreement. To explain the observed systematic

difference between the theory and the experiment, solid phase temperature measurements are needed.

SUMMARY AND CONCLUSIONS

(1) Infrared image analysis is an effective tool for studying phenomena associated with building fires. It can provide instantaneous measurement of two dimensional transient wall temperatures, and the pyrolysis–front spread rate in any direction can be deduced. Temporal pyrolysis front shapes on a PMMA surface for spreading fires were successfully measured by the IR technique.

(2) Total heat flux received on a PMMA sample surface was measured as a function of time for upwardly spreading fires at five height along the corner wall; approximately 50 – 60 % higher heat flux was measured for the corner fires in comparison to the flat vertical wall fires.

(3) The observed V–shaped pyrolysis front formation along the vertical corner wall is primarily due to the flame displacement effect near the corner walls.

(4) It was experimentally found that when the upward flame–spread pyrolysis–front reached near the ceiling, both downward spread from the ceiling to the pyrolysis front along the corner wall and horizontal spread along the ceiling occurred simultaneously. Because of this, a fire growth rate increased significantly.

(5) A simple prediction model for the maximum upward spread rate of pyrolysis front was proposed. The model is compared with the experimental data with a reasonable agreement. However, a further work is needed to explain the observed difference.

ACKNOWLEDGEMENTS

We wish to acknowledge Henry Mitler and Ken Steckler for their guidance in this research program, and John deRis and Forman Williams who offered helpful discussions which lead to the corner heat loss and convective cooling experiments, respectively. This study was supported by the National Institute of Standards and Technology through Grant No. 60NANB2D1295; Special Grants from Vice Chancellor's Office for Research and Graduate Studies; and the Center for Robotics and Manufacturing Systems, both are the University of Kentucky.

REFERENCES

[1] Orloff, L., deRis, J. and Markstein, G.H., "Upward Turbulent Fire Spread and Burning of Fuel Surface *Fifteenth Symposium (International) on Combustion,* The Combustion Institute, 1975, pp. 183–192.

[2] Mitler, H., "Predicting the Spread Rates of Fires on Vertical Surface," *Twenty–third Symposium (International) on Combustion,* The Combustion Institute, 1990, pp. 1715–1721.

[3] Saito, K. Quintiere, J.G., and Williams, F.A., Upward Turbulent Flame Spread," *Fire Safety Science – Proceedings of the First International Symposium,* Hemisphere Pub., 1985, pp. 75–86.

[4] Saito, K., Williams, F.A., Wichman, I.S., and Quintirere, J.G., *J. Heat Transfer,* 111:438 (1989).

[5] Quintiere, J.G., Harkleroad, M., and Hasemi, Y., *Combust. Sci. Tech.*, 48:191 (1986).

[6] Kulkalni, A.K., Kim, C.I., *Combust. Sci. Tech.,* 73:493 (1990).

[7] Delichatsios, M. and Saito, K., "Upward Flame Spread: Key Flammability Properties, Similarity Solutions and Flammability Indices," *Fire Safety Science – Procs. the Third International Symposium*, Elsevier Science Pub., 1991, pp. 217–226.

[8] Delichatsios, M.M, and Delichatsios, M.K., *Combustion and Flame*, 89:5 (1992).

[9] Williamson, R.B., Revenaugh, A., and Mower, F.W., "Ignition Sources in Room Fire Tests and Implications for Flame Spread Evaluation," *Fire Safety Science – Procs. the Third International Symposium,* Elsevier Science Pub., 1991, pp. .

[10] Daikoku, M., Lin, W.X. and Saito, K., "Visualization of Fire–Induced Flow", *Proc. the Central State Section, The Combustion Institute,* Nashville, TN, April, 1991.

[11] Arakawa, A., Saito, K., and Gruver, W.A., *Combust. Flame,* 92:222 (1992).

[12] Quintirere, J.G., "A Semi–Quantitative Model for the Burning Rate of Solid Materials," *NISTIR 4840,* Building and Fire Research Laboratory, National Institute of Standards and Technology, Gaithersburg, MD 20899, June, 1992.

[13] Roseman, R., Han, C.Y., Wee, W.G., and Murphy, J., "Classification of Infrared Images using Pattern Recognition and Artificial Neural Networks", *Proc. the Symposium on Advanced Manufacturing*, University of Kentucky, Lexington KY, Sept. 1989.

[14] Lyons, V., and Gracia–Salcedo, C.M., "Determination of Combustion Gas Temperatures by Infrared Radiometry in Sooting and Nonsooting Flames", *NASA AVSCOM Technical Report 88–C–008*, 1989.

[15] deRis, J., personal communication, 1992.

[16] Williams, F.A., personal communication, 1993.

[17] Qian, C., Isihda, H. and Saito, K., "Upward Flame Spread along the Vertical Corner Walls," *Proc. Central and Eastern States Section, The Combustion Institute,* New Orleans, LA, March, 1993.

[18] Qian, C. and Saito, K., "Fire–Induced Flow along the Vertical Corner Wall," *Proc. Asian Conference on Fire Science and Technology*, Heifei, China, 1992, pp. 257–262.

[19] Qian, C. and Saito, K., "Turbulent Flame Spread on Corner Walls," *Proc. of Eastern States Section: The Combustion Institute,* Princeton, NJ Oct. 25–27, 1993.

[20] Carslaw, H.S. and Jaeger, J.C., *Conduction of Heat in Solids*, 2nd Ed., Oxford, 1959.

Figures

Figure 1 A PMMA surface temperature history measured with a 0.07 mm diameter alumel–chromel thermocouple (TC) and IR camera (IR). Emissivity setup for the IR camera is one.

Figure 2 Schematics of experimental apparatus, flame shape and pyrolysis region visualized by an automated infrared imaging temperature measurement system.

Figure 3 Progress of pyrolysis front over a PMMA sample surface measure by IR camera with 10.8 ± 0.5 μm filter

Figure 4 (a) A schematic of flame shape after a spot ignition was applied at the bottom of PMMA corner, and (b) Pyrolysis front shape observed after flame was extinguished.

Figure 5 (a) A schematic of flame shape after one side of PMMA wall bottom was ignited, and (b) Pyrolysis front shape observed after the

Figure 6 Schematics of pyrolysis front shape on three different PMMA corner models (CASE I –III).

Figure 7 A schematic of pyrolysis front shape on a PMMA corner model surface with an aluminum square disc, 5 cm long x 5 cm wide x 0.2 cm thick.

Figure 8 Schematics of flame sheet location relative to corner wall surface (top view) and pyrolysis front shape on PMMA samples with four different corner angles. Figure (a): $\theta = 45^{o}$, (b): $\theta = 90^{o}$, (c): $\theta = 135^{o}$, and (d): $\theta = 180^{o}$.

Figure 9 (a) Photographs of the flames along the corner walls, and (b) IR images of the pyrolysis region at four different time periods after ignition.

Figure 10 Pyrolysis height as a function of time. Four different line ignition lengths were provided at the bottom of the PMMA corner walls.

Figure 11 Flame spread rate (= pyrolysis–front spread rate) as a function of pyrolysis height for three different ignition lengths.

Figure 12 (a) Pyrolysis shape measured by IR camera at six different time periods after ignition, and (b) a similarity correlation plot of pyrolysis shape.

Figure 13 Histories of total heat flux received at five different heights along the PMMA corner wall for a spreading fire.

Figure 14 Comparison of one–dimensional model, Eq. (5), of predicting pyrolysis height as a function of time with experimental data.

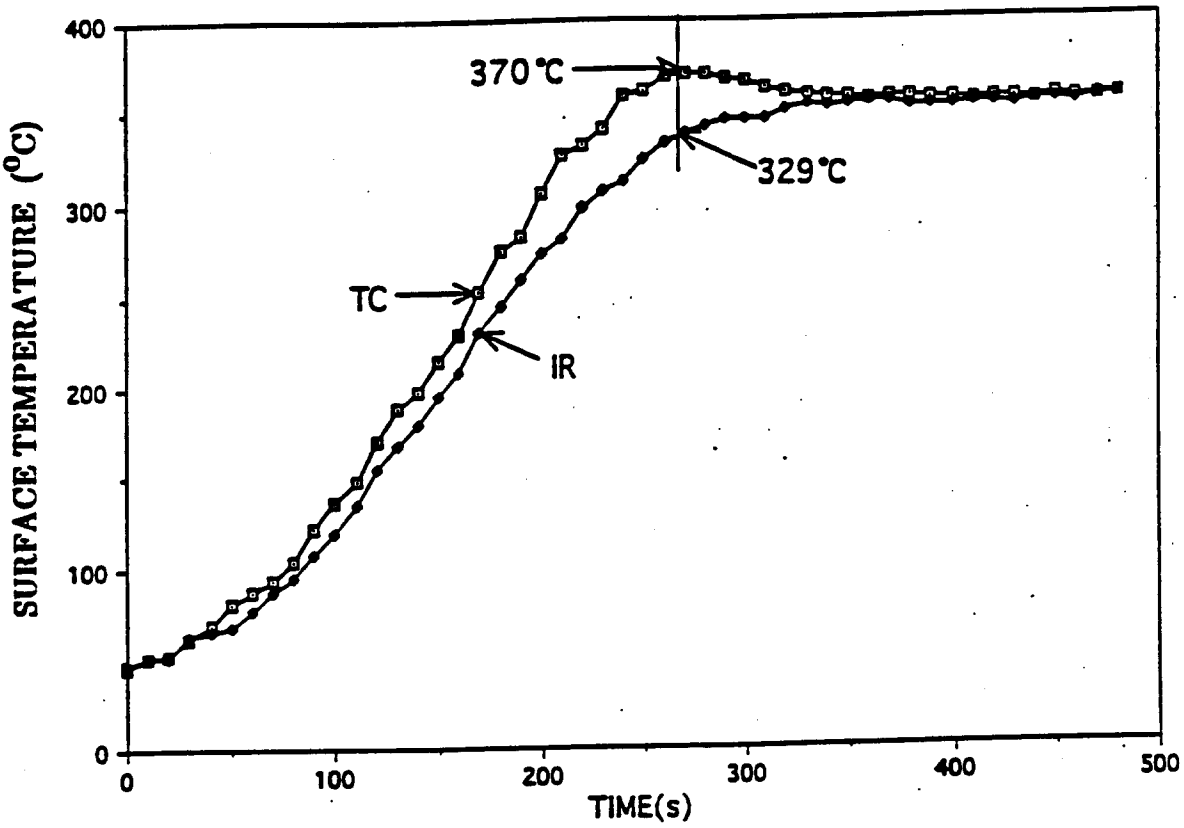

Figure 1 A PMMA surface temperature history measured with a 0.07 mm diameter alumel–chromel thermocouple (TC) and IR camera (IR). Emissivity setup for the IR camera is one.

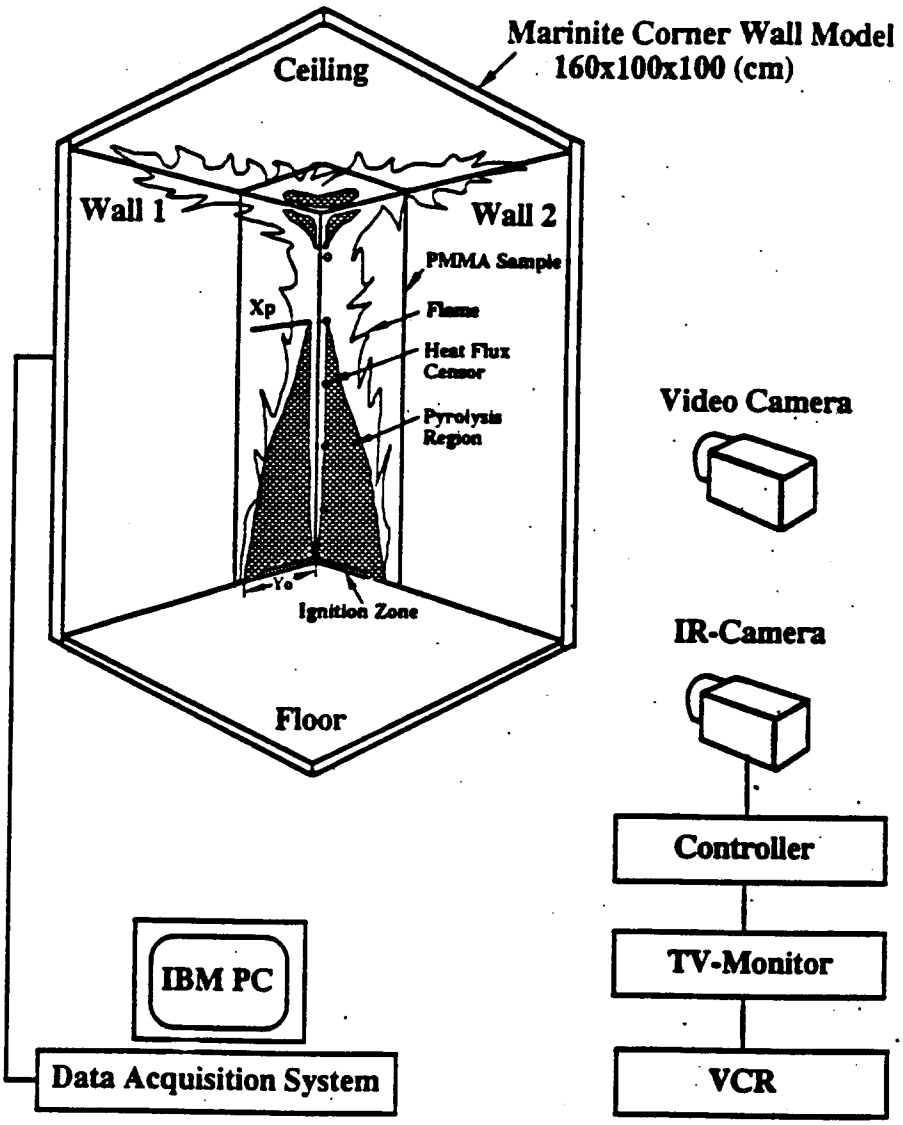

Figure 2 A schematic of experimental apparatus, flame shape and pyrolysis region visualized by an automated infrared imaging temperature measurement system.

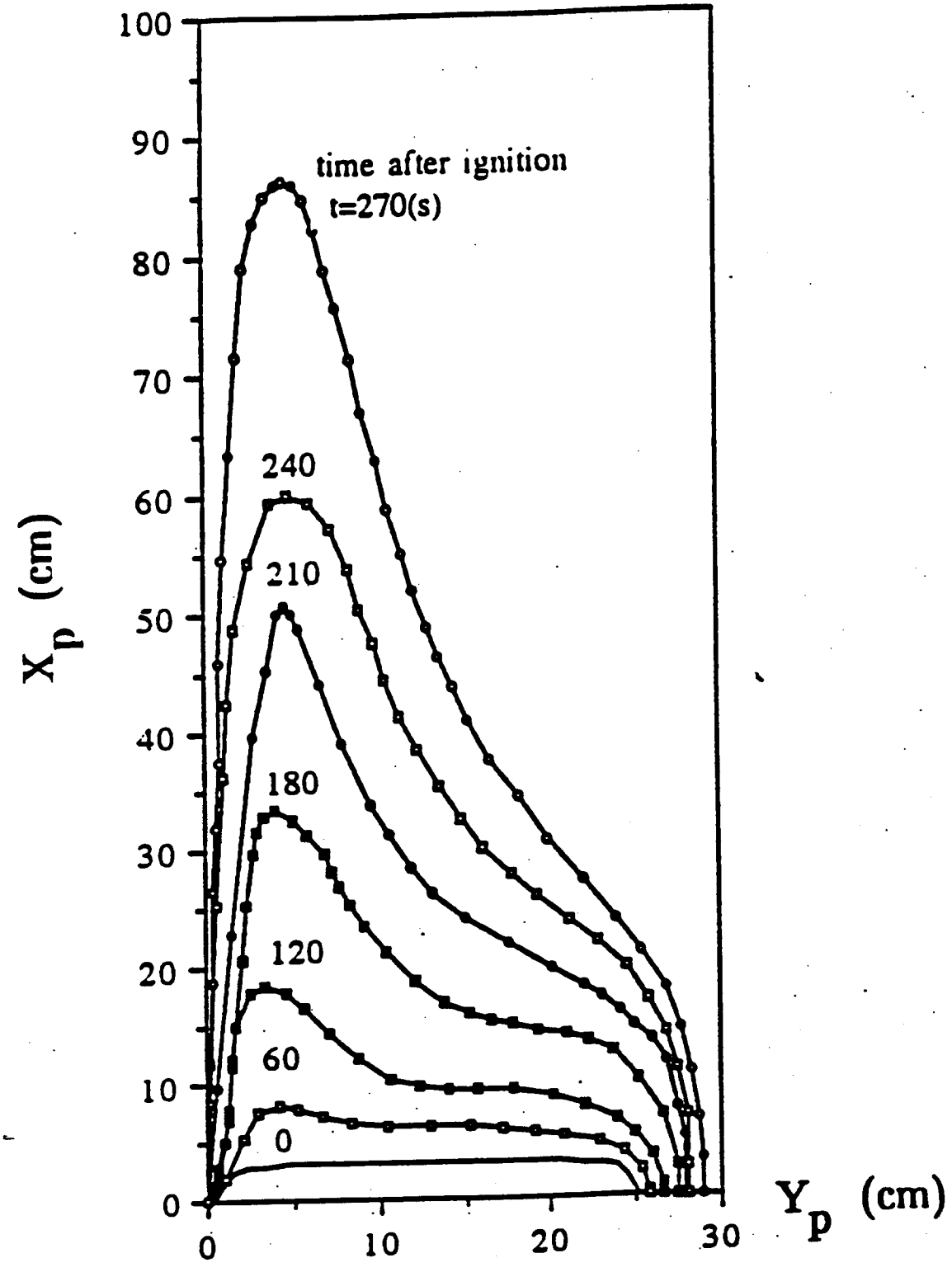

Figure 3 Progress of pyrolysis front over a PMMA sample surface measure by IR camera with 10.8 ± 0.5 μm filter

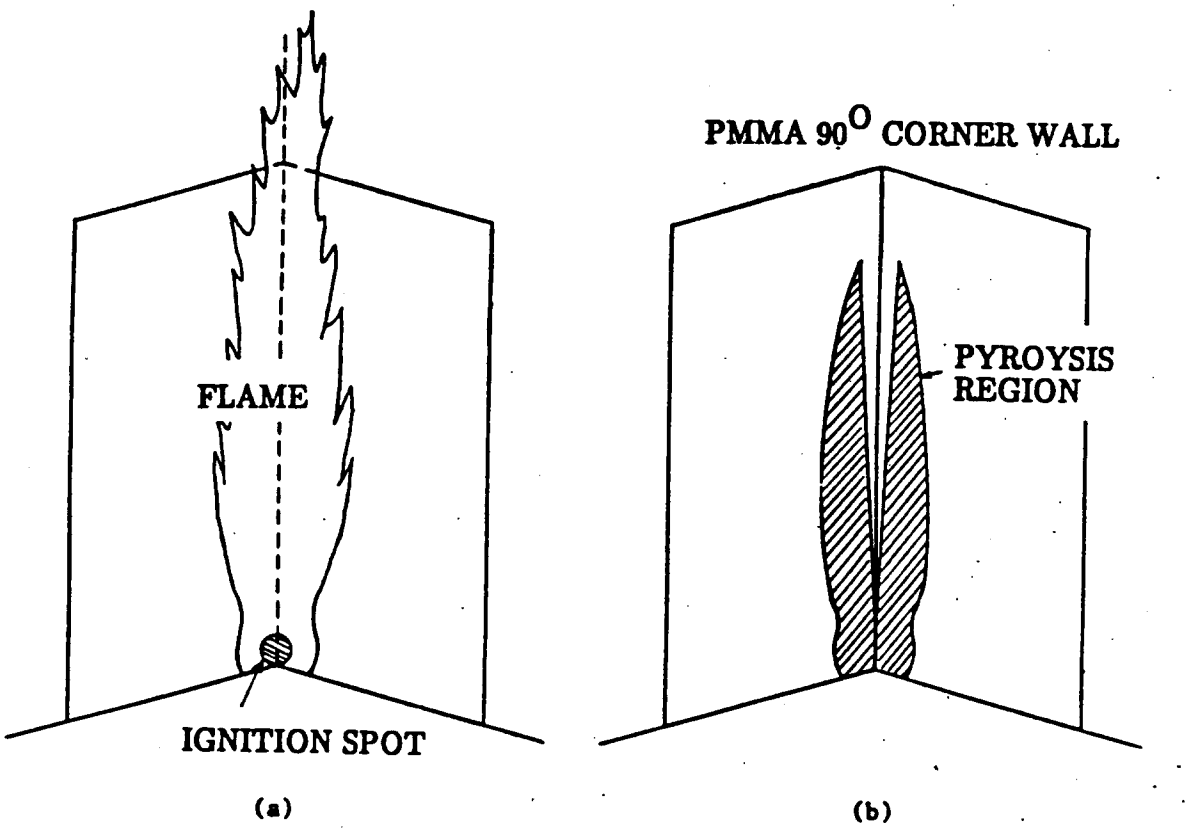

Figure 4 (a) A schematic of flame shape after a spot ignition was applied at the bottom of PMMA corner, and (b) Pyrolysis front shape observed after flame was extinguished.

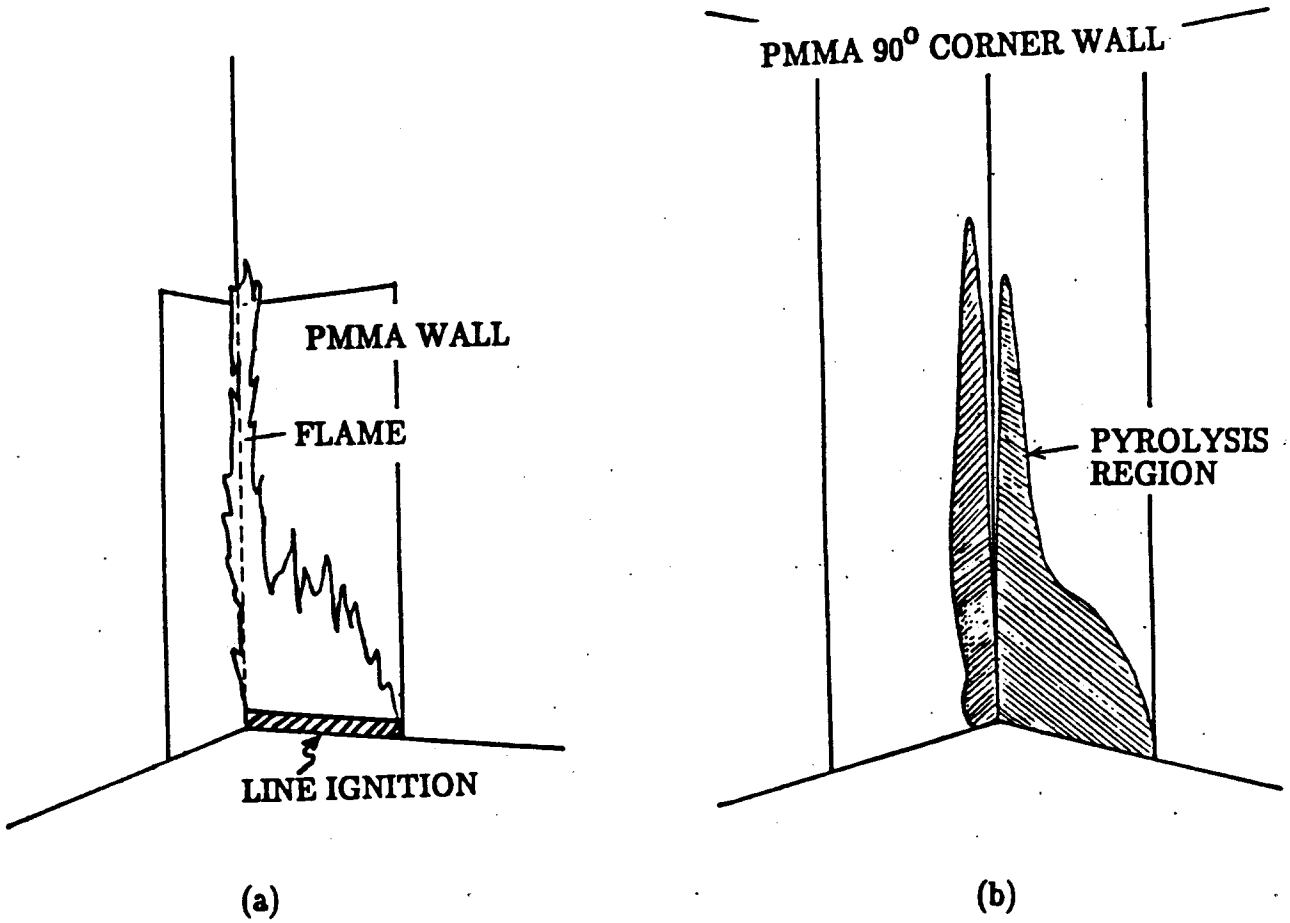

Figure 5 (a) A schematic of flame shape after one side of PMMA wall bottom was ignited, and (b) Pyrolysis front shape observed after the

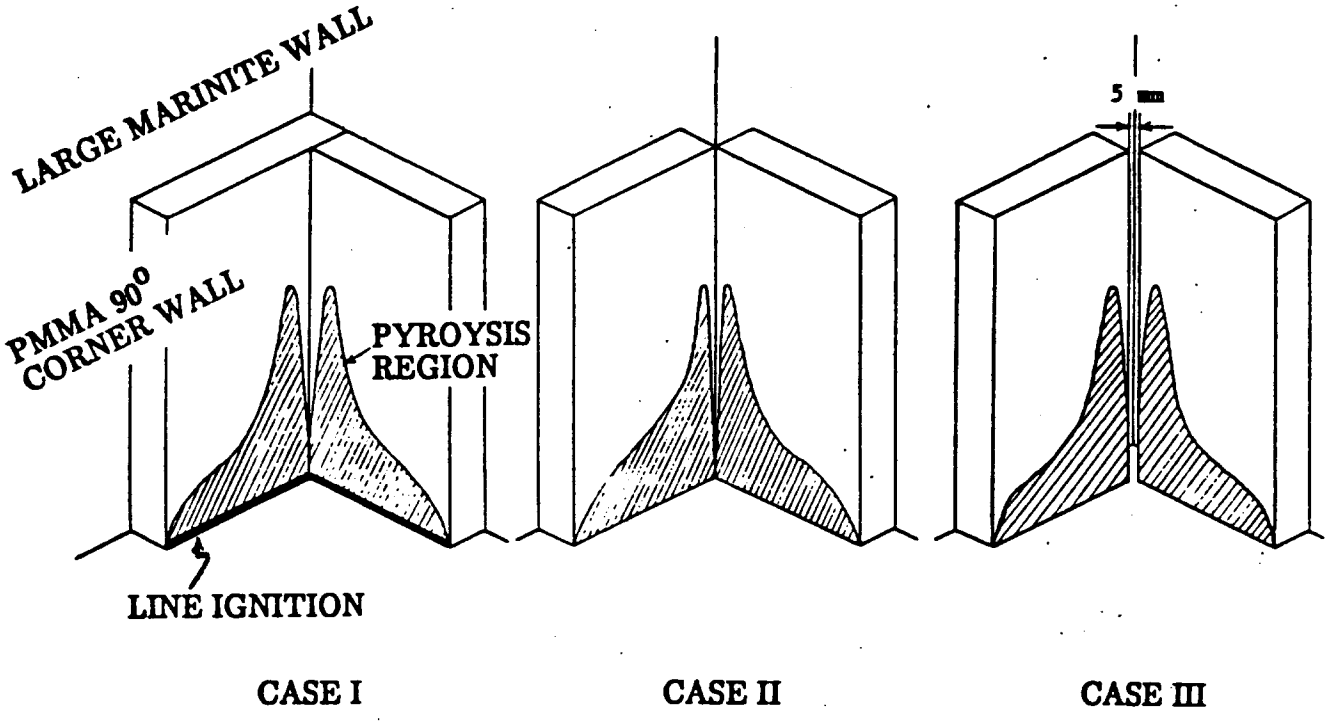

Figure 6 Schematics of pyrolysis front shape on three different PMMA corner models (CASE I –III).

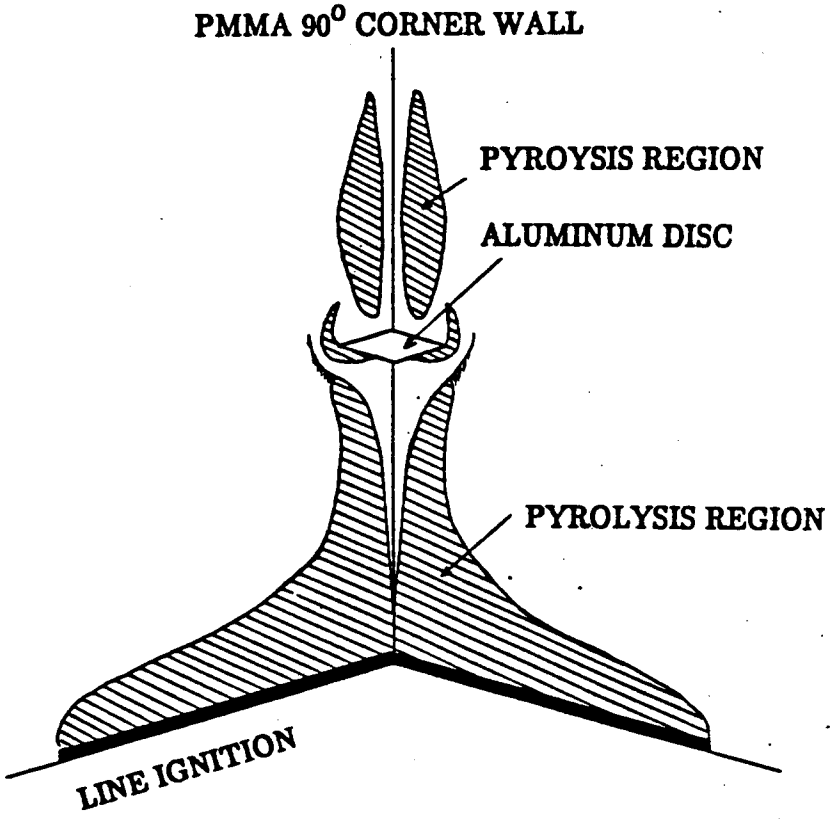

Figure 7 A schematic of pyrolysis front shape on a PMMA corner model surface with an aluminum square disc, 5 cm long x 5 cm wide x 0.2 cm thick.

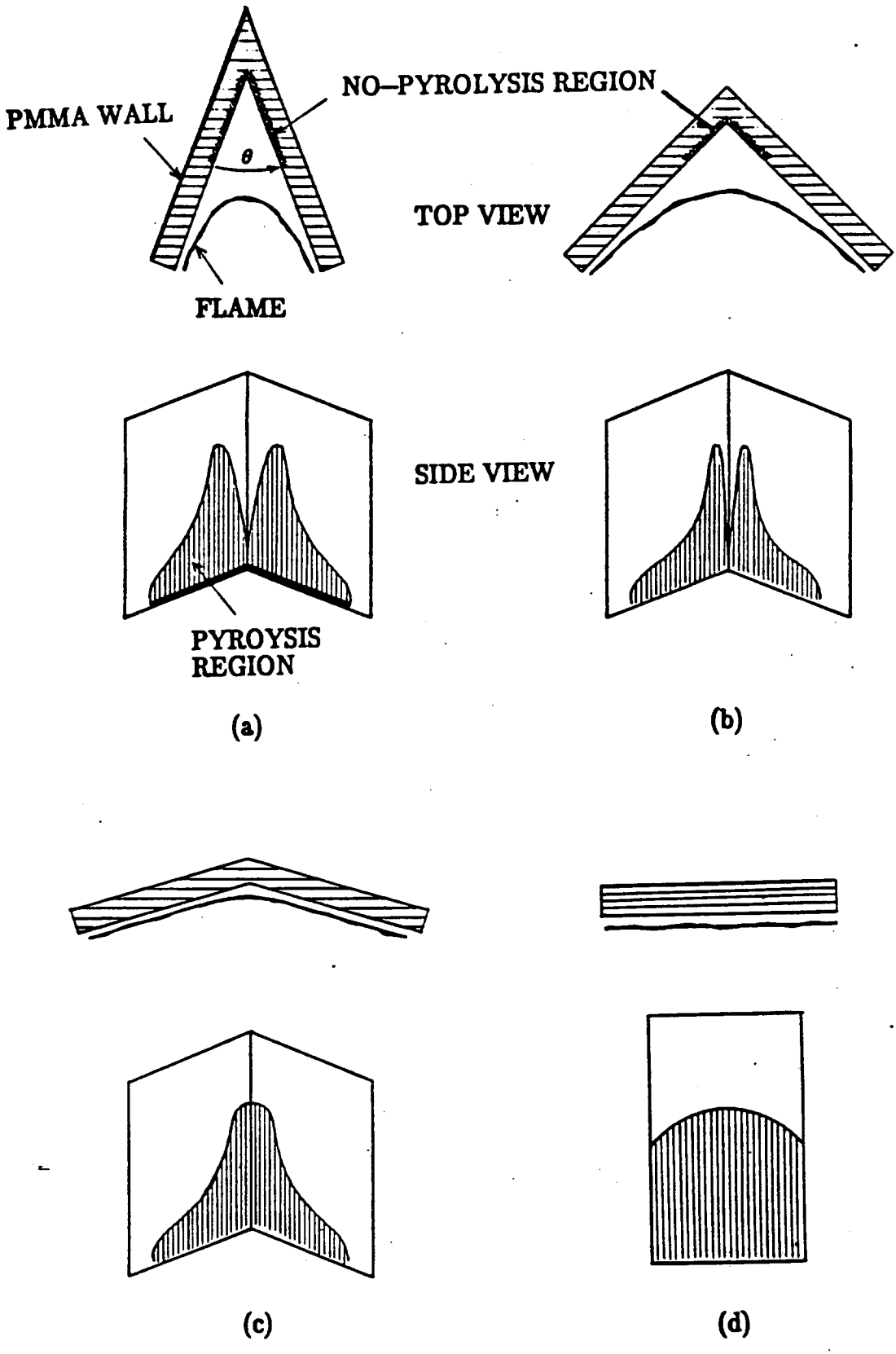

Figure 8 Schematics of flame sheet location relative to corner wall surface (top view) and pyrolysis front shape on PMMA samples with four different corner angles. Figure (a): $\theta = 45^{o}$, (b): $\theta = 90^{o}$, (c): $\theta = 135^{o}$, and (d): $\theta = 180^{o}$.

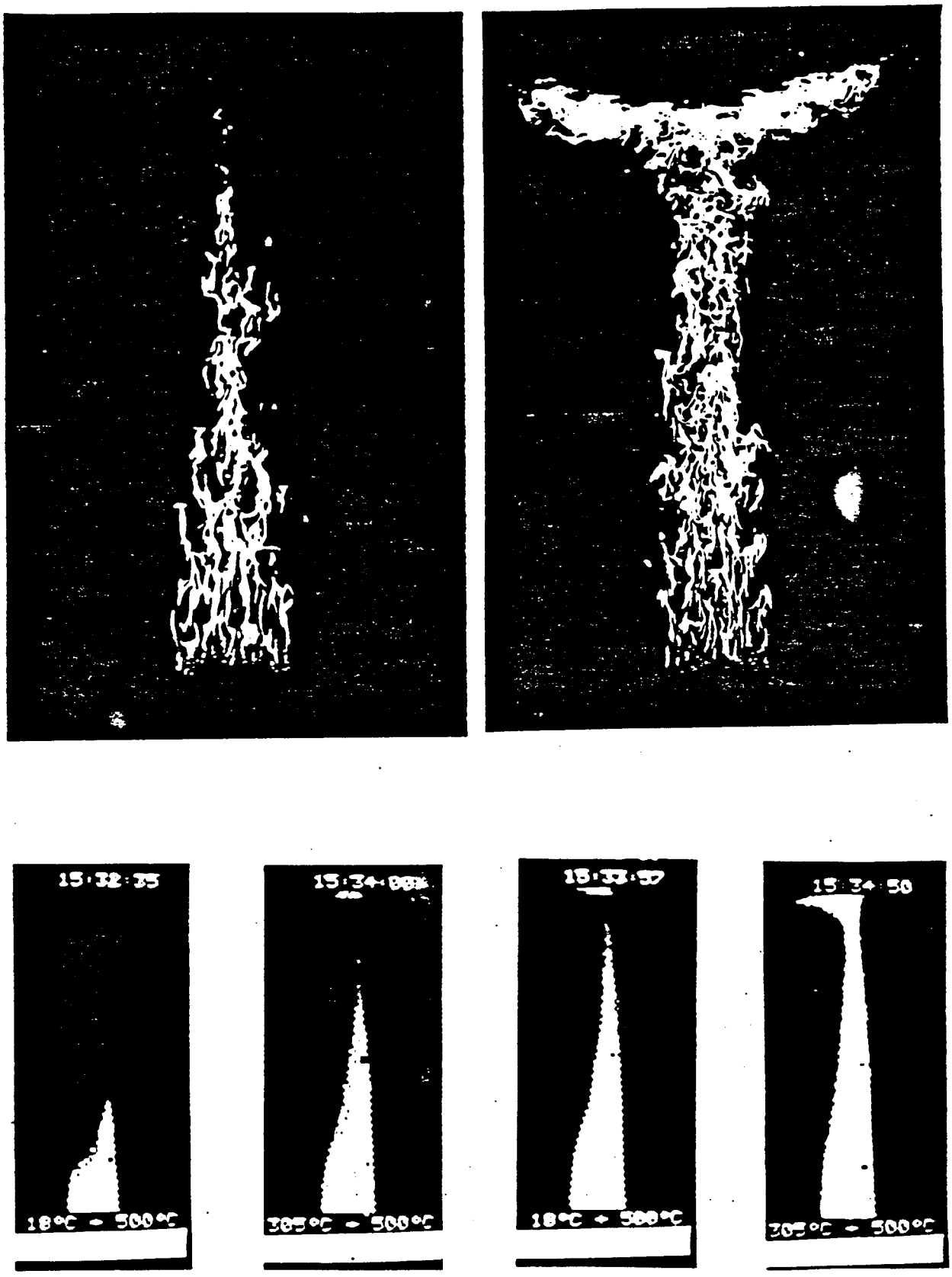

Figure 9 (a) Photographs of the flames along the corner walls, and (b) IR images of the pyrolysis region at four different time periods after ignition.

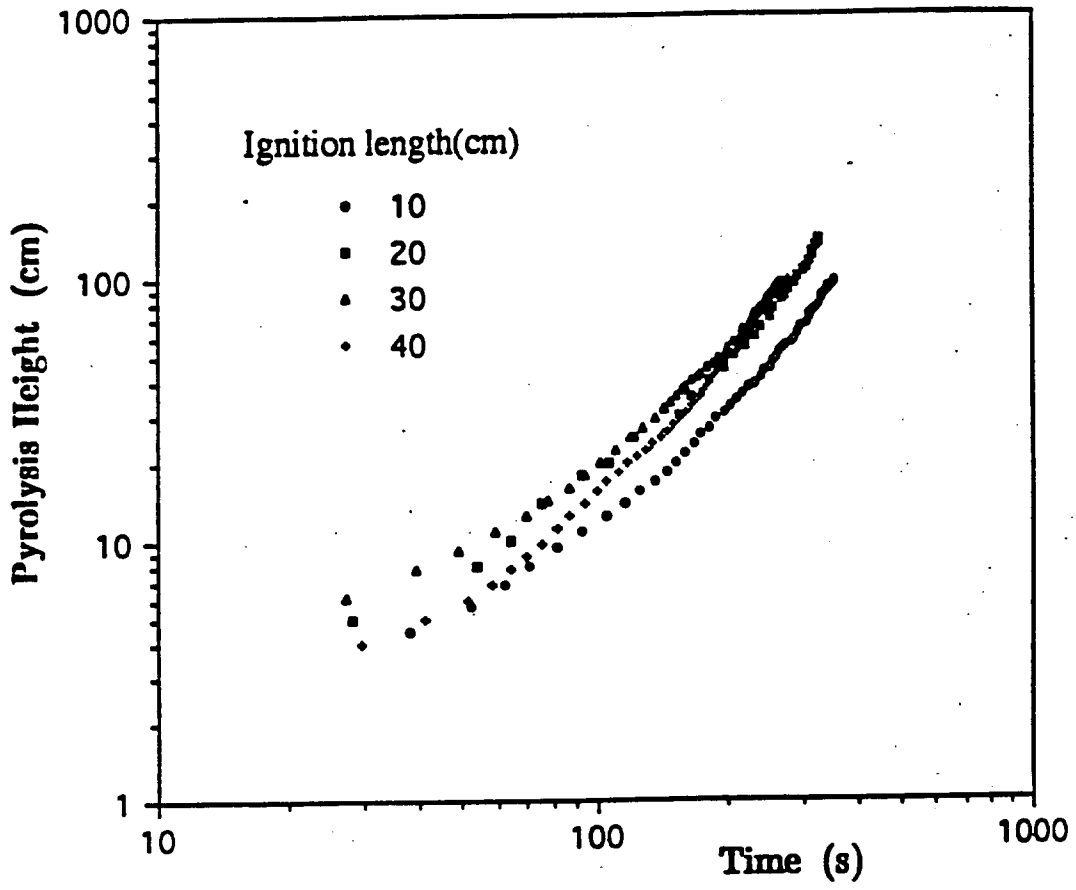

Figure 10 Pyrolysis height as a function of time. Four different line ignition lengths were provided at the bottom of the PMMA corner walls.

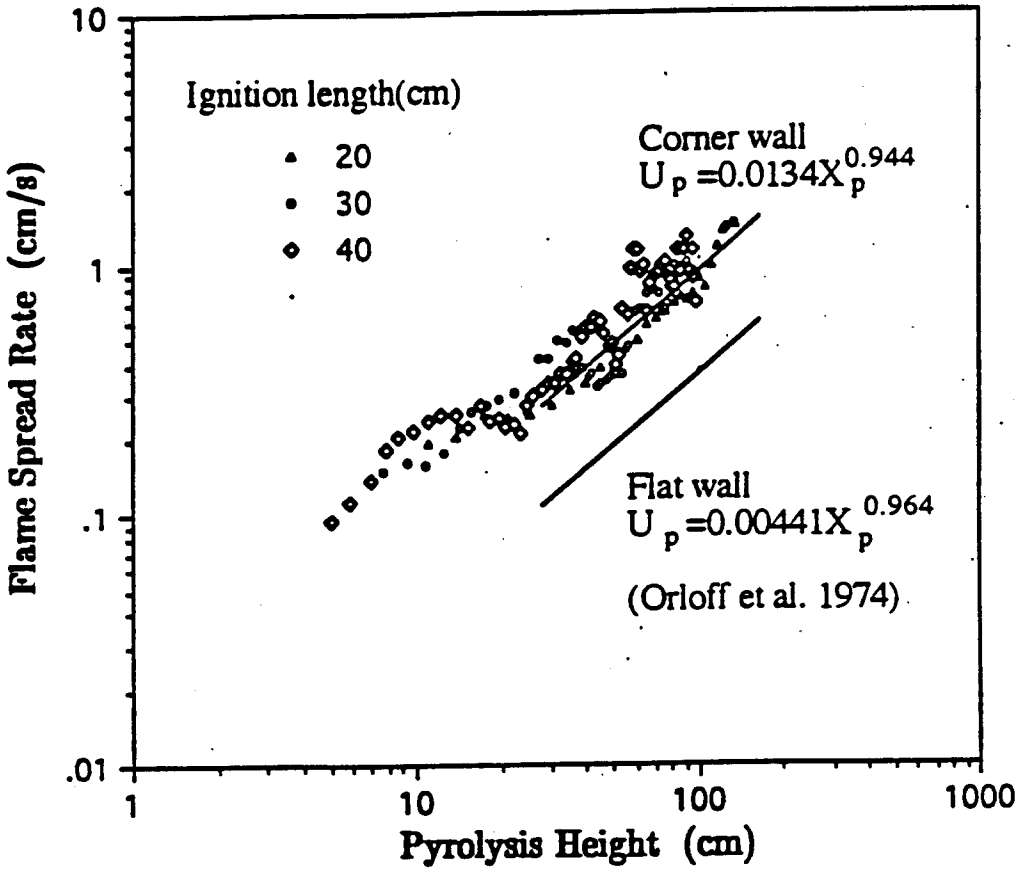

Figure 11 Flame spread rate (= pyrolysis–front spread rate) as a function of pyrolysis height for three different ignition lengths.

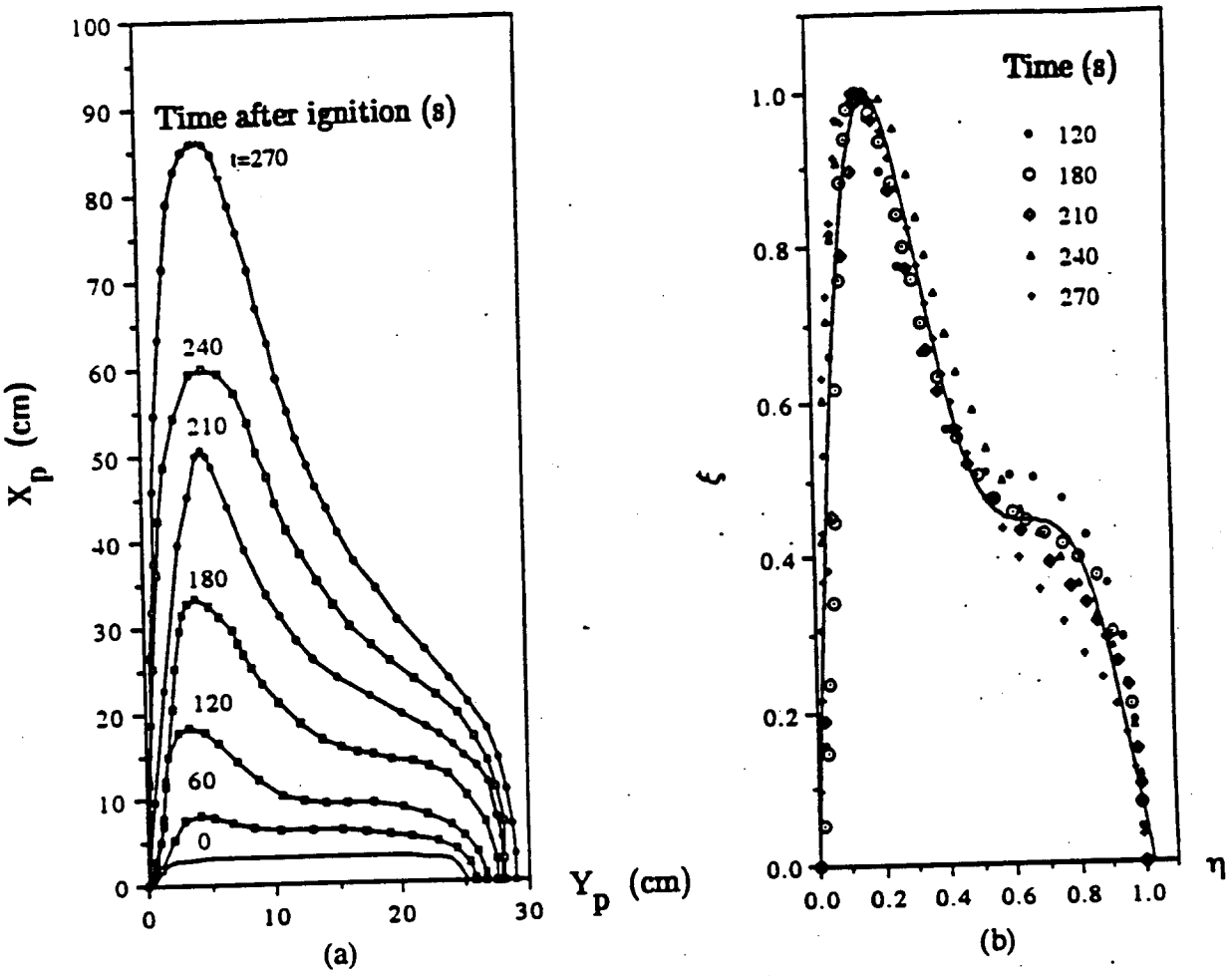

Figure 12 (a) Pyrolysis shape measured by IR camera at six different time periods after ignition, and (b) a similarity correlation plot of pyrolysis shape.

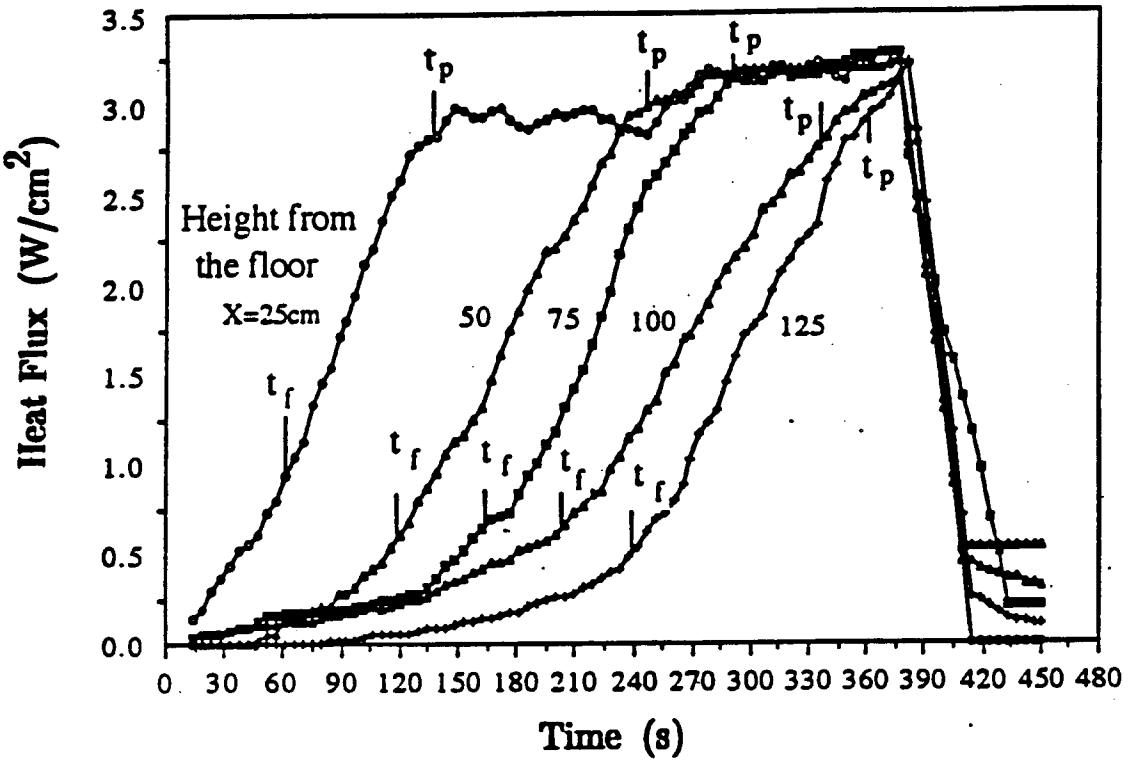

Figure 13 Histories of total heat flux received at five different heights along the PMMA corner wall for a spreading fire.

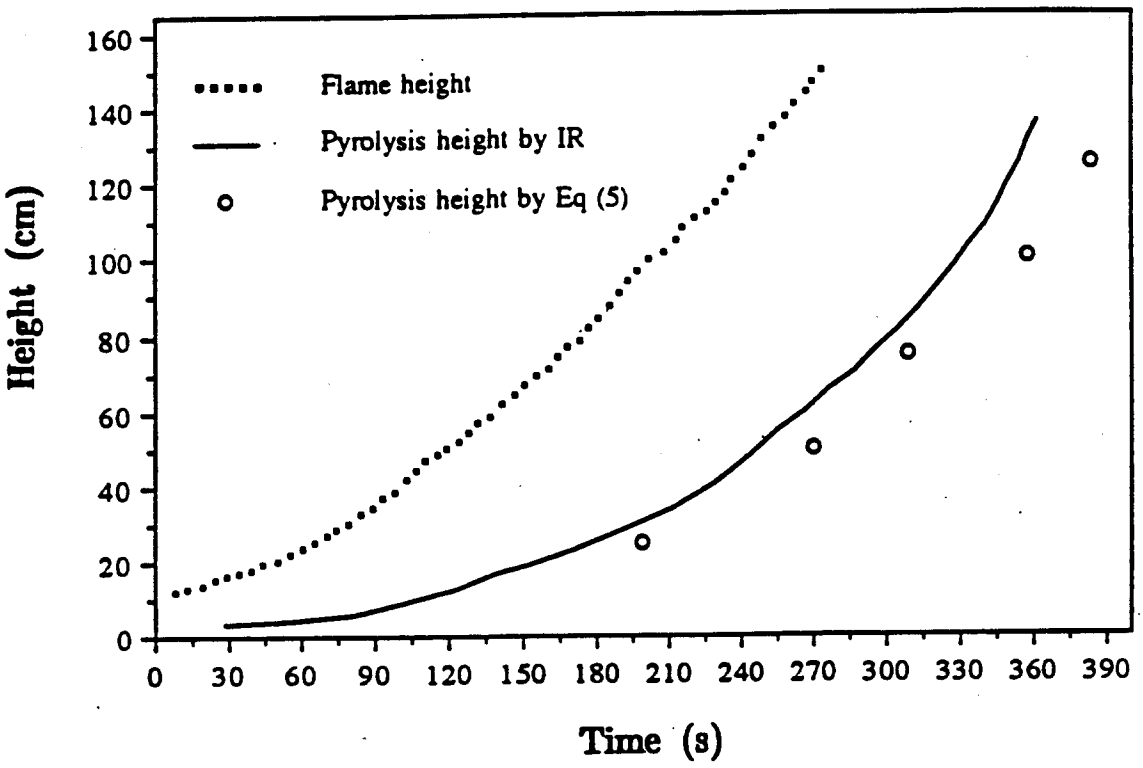

Figure 14 Comparison of one–dimensional model, Eq. (5), of predicting pyrolysis height as a function of time with experimental data.

APPENDIX

Heat Flux and Temperature Distributions on a Corner Wall With and Without Ceiling

A series of heat flux and temperature distribution measurements were performed using our one–half scale room corner model. Corner walls and floor were made of a 1.5 cm thick Marinite board. One case Marinite ceiling was placed on the top of corner walls and another case no ceiling was placed. A propane gas burner, 15 cm long x 15 wide x 5 cm high, was placed on the floor near the corner. Both temperature and heat flux measurements were performed after a steady state temperature distribution was achieved on the wall. Total heat flux was measured with three water–cooled heat flux gauges; the two flux meters were fixed on specified the corner wall locations to provide reference temperatures, while one flux meter was traversed from point to point. The locations that those measurements were performed are shown in Fig. A1. Temperature distribution measurements were performed with the IR camera as the main device and the thermocouples as a supplement device.

Two different burner heat release rates (13.5 and 18 kW) were used and six different burner stand–off distance (0, 2.5, 5, 10, 15 and 20 cm) were used. Heat flux and temperature distributions with the ceiling case are compared with those without the ceiling case at the same burner heat flux and burner stand–off distance conditions. The heat flux and temperature distributions on a corner wall are shown in Figs. 2A through 5A, while the temperature distributions on the ceiling are shown in Fig. 6A. Interestingly, both the heat flux and temperature distributions with the ceiling case are lower than those without the ceiling case. It may be because that the ceiling is a resistance for the fire–induced flow causing a stagnation near the corner wall surface. Because of this, the convective heat feedback to the wall decreased.

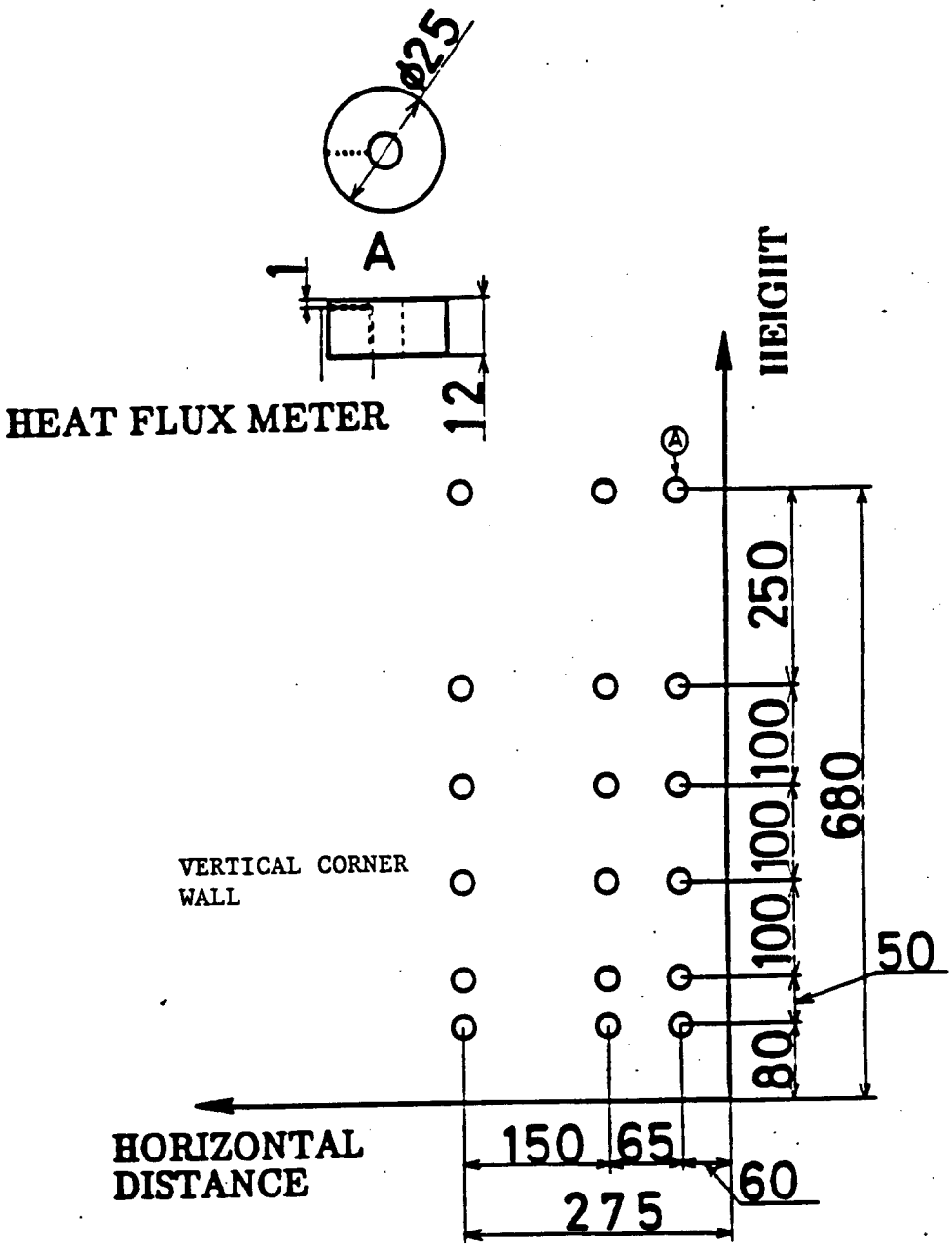

Fig. A1 Measurement locations for the total heat flux distributions on the Marinite wall (unit: mm).

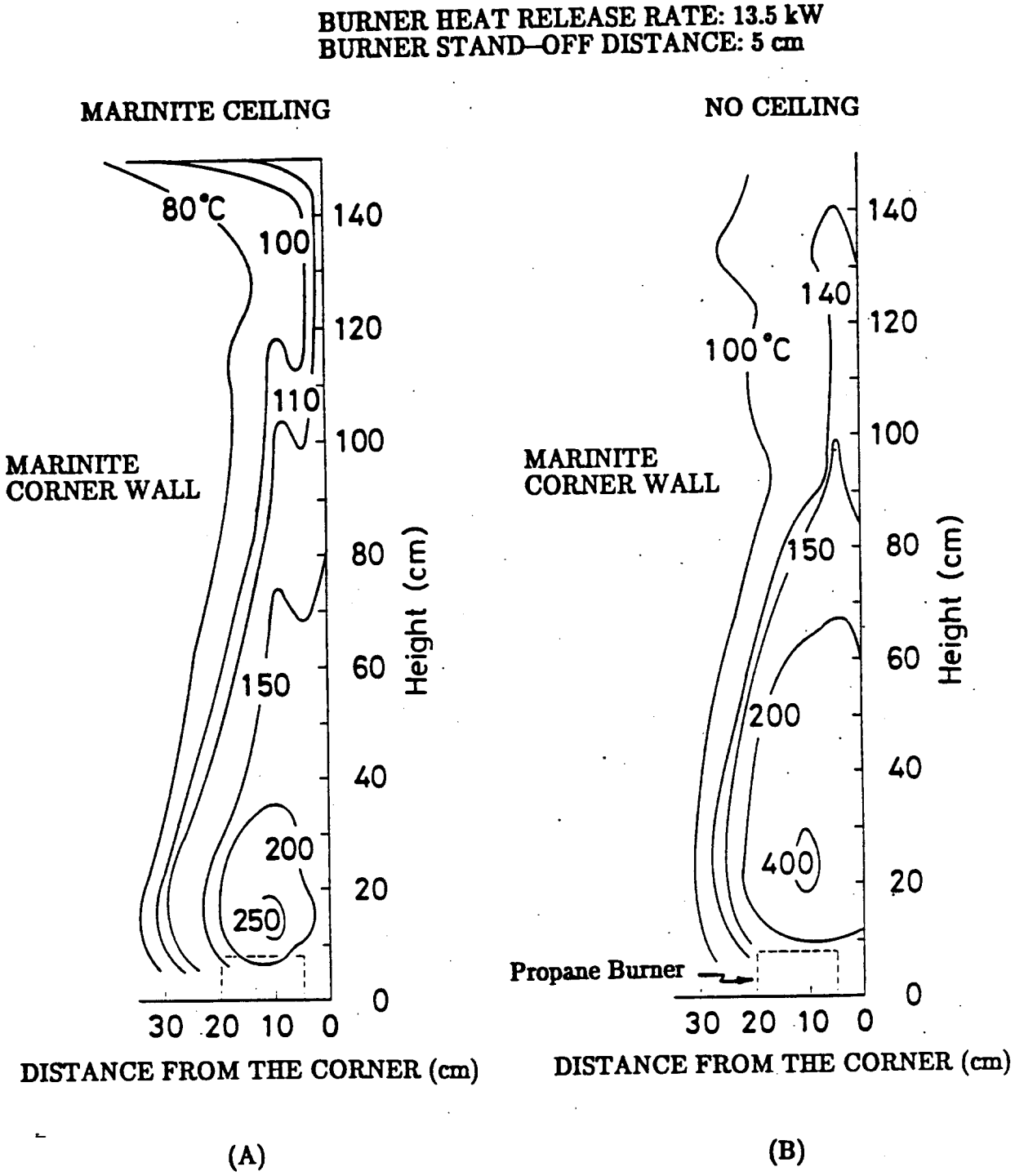

Fig. A2 Temperature profiles on a fire–heated Marinite vetical corner wall. (A: with a Marinite ceiling; B: with no ceiling).

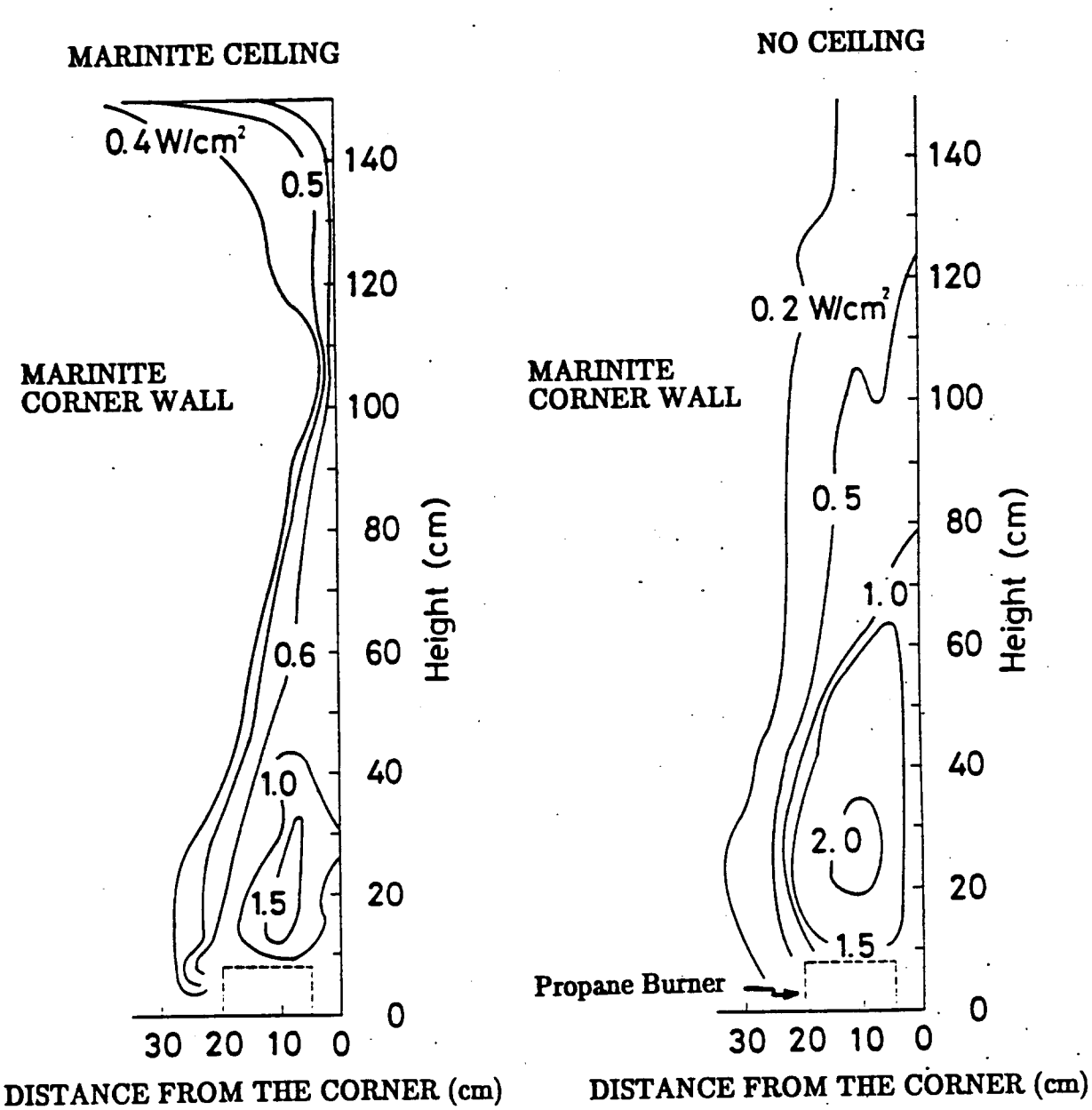

Fig. A3 Total heat flux distribution on a fire–heated Marinite corner wall. (A: with a Marinite ceiling; B: with no ceiling).

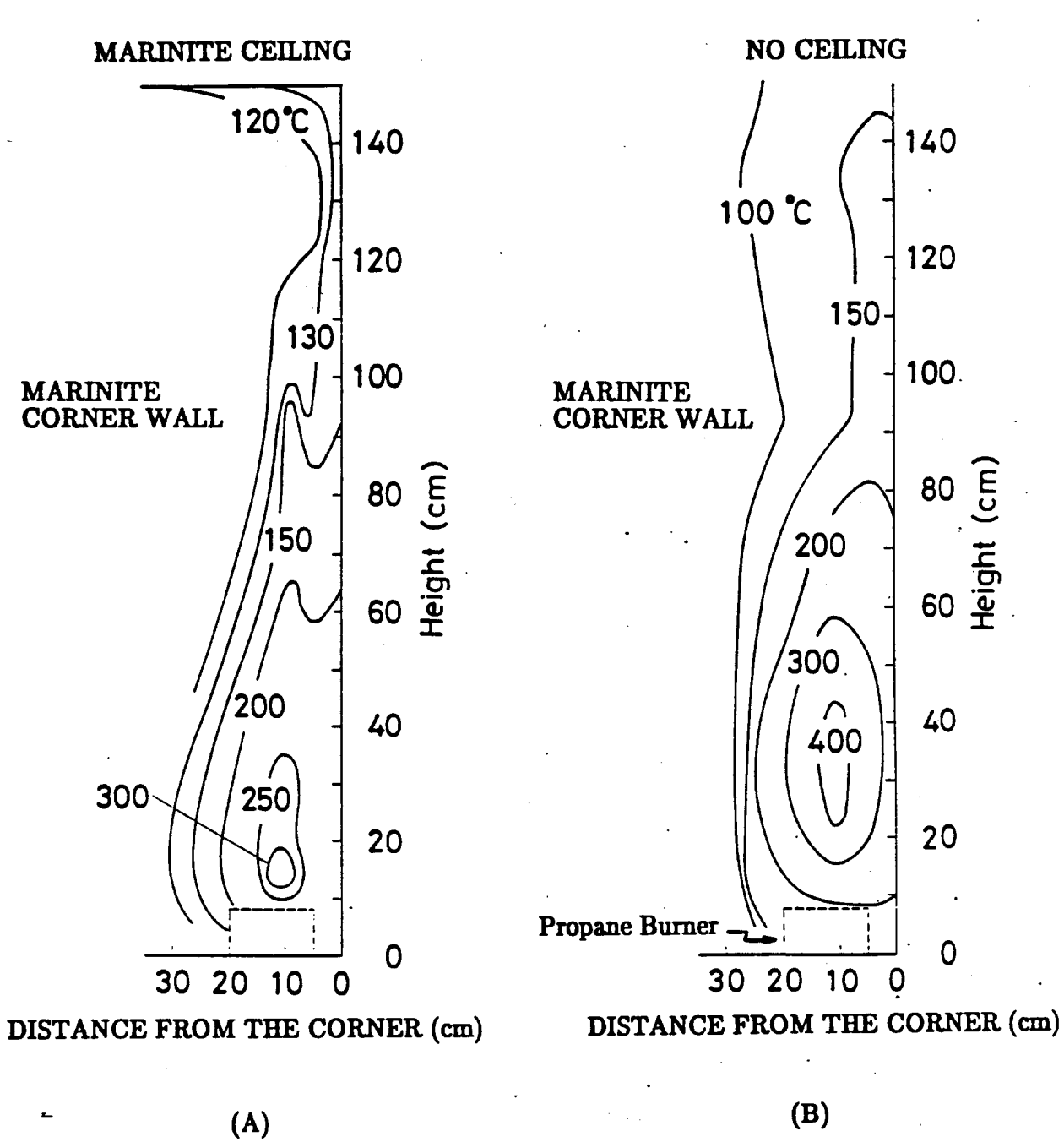

Fig. A4 Temperature profiles on a fire–heated Marinite vertical corner wall. (A: with a Marinite ceiling; B: with no ceiling).

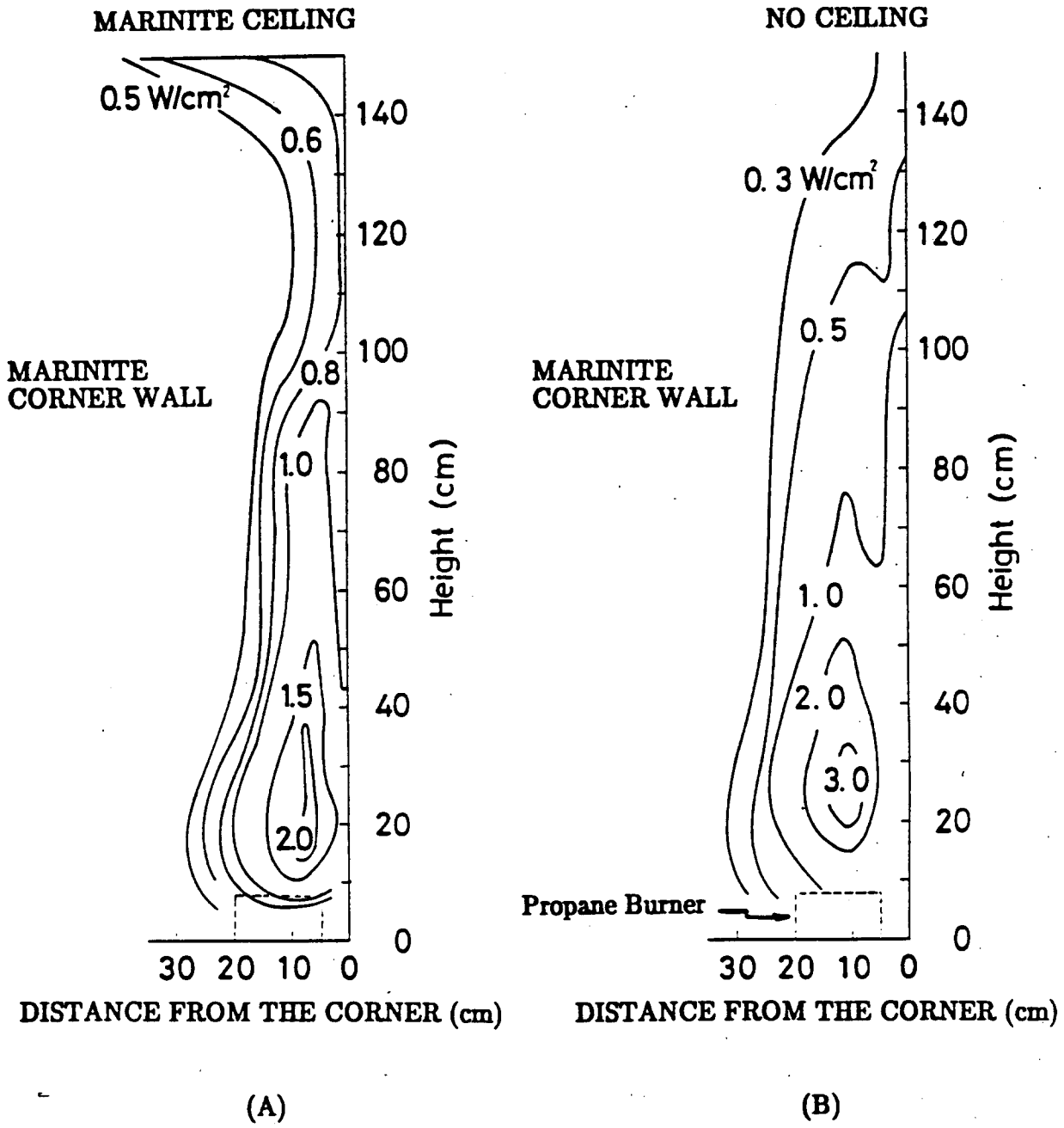

Fig. A5 Total heat flux distribution on a fire–heated Marinite corner wall. (A: with a Marinite ceiling; B with no ceiling).

BURNER HEAT RELEASE RATE: 13.5kW

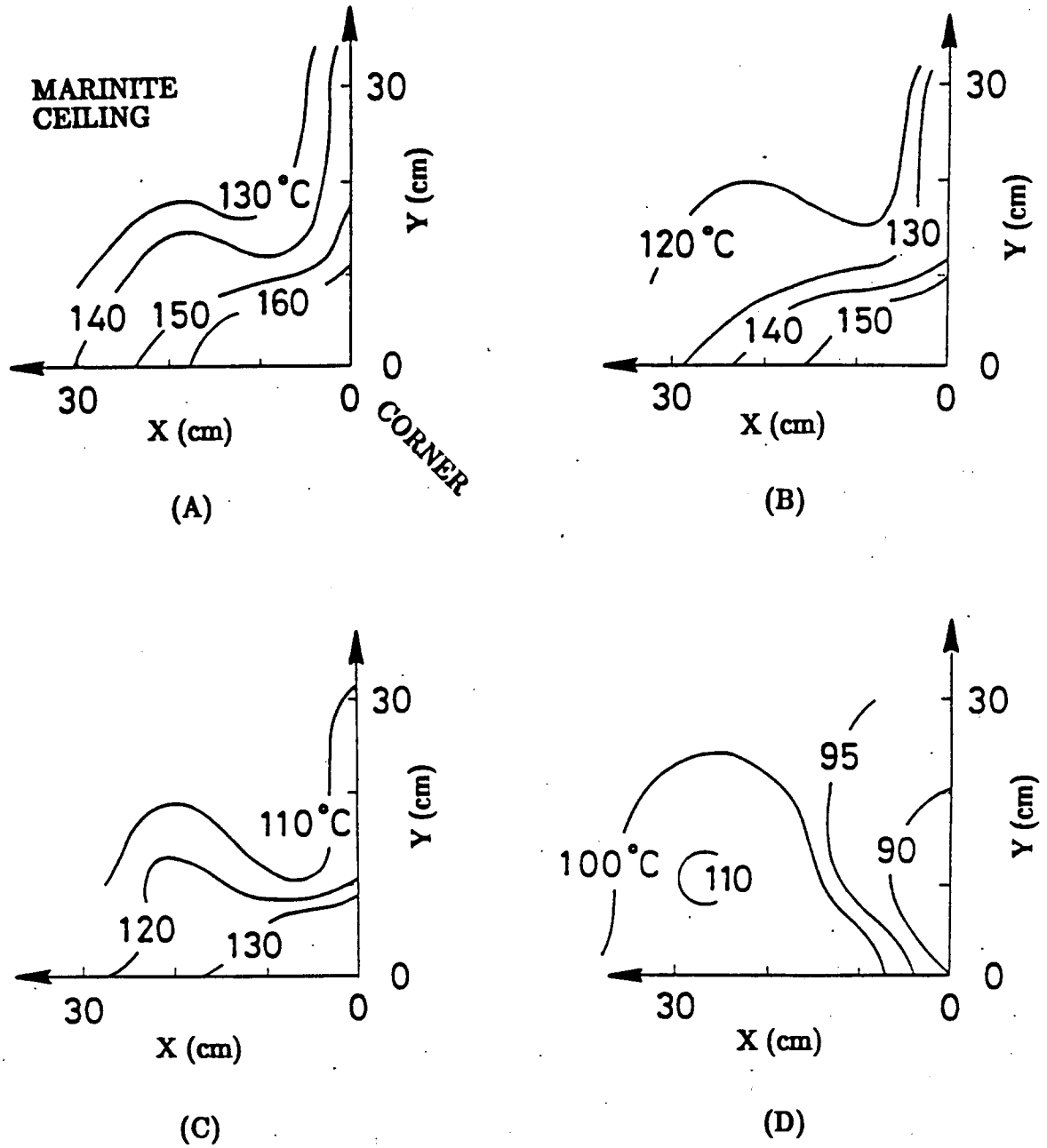

Fig. A6 Temperature profiles on a fire–heated Marinite corner ceiling. (A: burner stand–off distance, L = 0; B: L = 2.5 cm; C: L = 5 cm; D = 10 cm).

NIST-114
(REV. 9-92)
ADMAN 4.09

U.S. DEPARTMENT OF COMMERCE
NATIONAL INSTITUTE OF STANDARDS AND TECHNOLOGY

MANUSCRIPT REVIEW AND APPROVAL

(ERB USE ONLY)
ERB CONTROL NUMBER | DIVISION
PUBLICATION REPORT NUMBER: NIST-GCR-94-648 | CATEGORY CODE

INSTRUCTIONS: ATTACH ORIGINAL OF THIS FORM TO ONE (1) COPY OF MANUSCRIPT AND SEND TO: THE SECRETARY, APPROPRIATE EDITORIAL REVIEW BOARD.

PUBLICATION DATE: June 1994 | NUMBER PRINTED PAGES

TITLE AND SUBTITLE (CITE IN FULL)
Upward Flame Spread Along the Vertical Corner Walls

CONTRACT OR GRANT NUMBER
60NANB2D1295

TYPE OF REPORT AND/OR PERIOD COVERED
Final Report October 14, 1993

AUTHOR(S) (LAST NAME, FIRST INITIAL, SECOND INITIAL)
Kozo Saito
University of Kentucky
Department of Mechanical Engineering
Lexington, KY 40506-0108

PERFORMING ORGANIZATION (CHECK (X) ONE BOX)
[ ] NIST/GAITHERSBURG
[ ] NIST/BOULDER
[ ] JILA/BOULDER

LABORATORY AND DIVISION NAMES (FIRST NIST AUTHOR ONLY)

SPONSORING ORGANIZATION NAME AND COMPLETE ADDRESS (STREET, CITY, STATE, ZIP)
U.S. Department of Commerce
National Institute of Standards and Technology
Gaithersburg, MD 20899

RECOMMENDED FOR NIST PUBLICATION
[ ] JOURNAL OF RESEARCH (NIST JRES)
[ ] J. PHYS. & CHEM. REF. DATA (JPCRD)
[ ] HANDBOOK (NIST HB)
[ ] SPECIAL PUBLICATION (NIST SP)
[ ] TECHNICAL NOTE (NIST TN)
[ ] MONOGRAPH (NIST MN)
[ ] NATL. STD. REF. DATA SERIES (NIST NSRDS)
[ ] FEDERAL INF. PROCESS. STDS. (NIST FIPS)
[ ] LIST OF PUBLICATIONS (NIST LP)
[ ] NIST INTERAGENCY/INTERNAL REPORT (NISTIR)
[ ] LETTER CIRCULAR
[ ] BUILDING SCIENCE SERIES
[ ] PRODUCT STANDARDS
[ ] OTHER NIST-GCR-

RECOMMENDED FOR NON-NIST PUBLICATION (CITE FULLY) [ ] U.S. [ ] FOREIGN

PUBLISHING MEDIUM
[ ] PAPER [ ] CD-ROM
[ ] DISKETTE (SPECIFY)
[ ] OTHER (SPECIFY)

SUPPLEMENTARY NOTES

ABSTRACT (A 1500-CHARACTER OR LESS FACTUAL SUMMARY OF MOST SIGNIFICANT INFORMATION. IF DOCUMENT INCLUDES A SIGNIFICANT BIBLIOGRAPHY OR LITERATURE SURVEY, CITE IT HERE. SPELL OUT ACRONYMS ON FIRST REFERENCE.) (CONTINUE ON SEPARATE PAGE, IF NECESSARY.)

Flame spread behavior and the pyrolysis region spread characteristics along vertical corner walls were studied in detail with an automated infrared imaging temperature measurement technique (IR technique). The technique was recently developed for the measurement of transient pyrolysis temperature on both charring and non-charring materials. Temporal isotherms on PMMA samples were successfully obtained, from which the progress rate of the pyrolysis front was automatically deduced. It was found that the pyrolysis front shape was always M-shaped, i.e., no spread along the corner, and the maximum spread is in a few centimeters away from the corner. Understanding of the mechanism of the M-shape formation is important in developing a prediction model of the spread rate. Four possible mechanisms were identified and flame displacement effects are found to be the principal mechanism. Transient total heat flux distributions above the M-shape pyrolysis peak for a spreading fire were measured. Using these values, it was shown that the upward spread rate is predictable from a simple, one-dimensional, thermal model.

KEY WORDS (MAXIMUM 9 KEY WORDS; 28 CHARACTERS AND SPACES EACH; ALPHABETICAL ORDER; CAPITALIZE ONLY PROPER NAMES)
corners; flame spread; heat flux; polymethylmethacrylate; pyrolysis; walls

AVAILABILITY
[X] UNLIMITED [ ] FOR OFFICIAL DISTRIBUTION. DO NOT RELEASE TO NTIS.
[ ] ORDER FROM SUPERINTENDENT OF DOCUMENTS, U.S. GPO, WASHINGTON, D.C. 20402
[X] ORDER FROM NTIS, SPRINGFIELD, VA 22161

NOTE TO AUTHOR(S) IF YOU DO NOT WISH THIS MANUSCRIPT ANNOUNCED BEFORE PUBLICATION, PLEASE CHECK HERE. [ ]

ELECTRONIC FORM